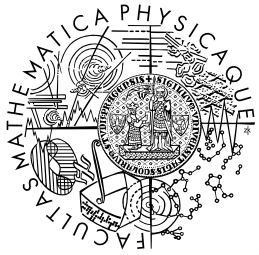

FACULTY
OF MATHEMATICS
AND PHYSICS
Charles University

BACHELOR THESIS

Martin Vavřík

Simulation and Reconstruction of Charged Particle Trajectories in an Atypic Time Projection Chamber

Institute of Particle and Nuclear Physics

Supervisor of the bachelor thesis: Mgr. Tomáš Sýkora, Ph.D.

Study programme: Physics

Prague 2025

I declare that I carried out this bachelor thesis independently, and only with the cited sources, literature and other professional sources. It has not been used to obtain another or the same degree.

I understand that my work relates to the rights and obligations under the Act No. 121/2000 Sb., the Copyright Act, as amended, in particular the fact that the Charles University has the right to conclude a license agreement on the use of this work as a school work pursuant to Section 60 subsection 1 of the Copyright Act.

In ..... date ....

Author's signature

16 Dedication.

Title: Simulation and Reconstruction of Charged Particle Trajectories in an Atypic Time Projection Chamber Added hyphen to avoid overfull hbox

Author: Martin Vavřík

Institute: Institute of Particle and Nuclear Physics

Supervisor: Mgr. Tomáš Sýkora, Ph.D., Institute of Particle and Nuclear Physics

Abstract: Abstract.

Keywords: key words

Contents

Motivation

A Time Projection Chamber (TPC) is a type of gaseous detector that detects charged particle trajectories by measuring the positions and drift time of ions created in the gas; details are provided in Section 1. The energy of these particles can be inferred from the curvature of their trajectory in the magnetic field.

The goal of this thesis is to develop an algorithm for the reconstruction of charged particle trajectories and energy in an atypic TPC with orthogonal electric and magnetic fields, hereafter referred to as the Orthogonal Fields TPC (OFTPC), used in the X17 project at the Institute of Experimental and Applied Physics, Czech Technical University in Prague (IEAP CTU). Furthermore, we present the results of testing this algorithm with different samples of simulated data. (We use the Garfield++ toolkit [1] for simulations in combination with the ROOT framework [2] for data analysis and visualization. Some of our more demanding simulations are run on the MetaCentrum grid [3].)

The X17 project in IEAP CTU aims to reproduce measurements of anomalous behavior in the angular correlation distribution of pairs produced by the Internal Pair Creation (IPC) mechanism [4] during the decay of certain excited nuclei (^{8}Be, ^{12}C, and ^{4}He) observed by a team at ATOMKI in Hungary. I would leave this here as a short summary before I explain it in more detail in the sections below.

Add citations: X17 project, VdG. Maybe also TPC, etc.

0.1 ATOMKI Anomaly

0.1.1 ATOMKI Measurements

In 2015 a group at ATOMKI led by Attila Krasznahorkay observed an anomalous Internal Pair Creation in ^{8}Be while attempting to find a new light neutral boson [5]. They used the $^{7}\mathrm{Li}(p,\gamma)^{8}\mathrm{Be}$ reaction at the $E_p = 1030$ keV proton capture resonance to prepare the 18.15 MeV excited state ($J^\pi = 1^+$, $T = 0$). This state decays predominantly through M1 transitions to the ground state ($J^\pi = 0^+$, $T = 0$) and to the 3.03 MeV state ($J^\pi = 2^+$, $T = 0$) [6].

The angular correlation of the e^+e^- pairs created internally in these transitions were measured and compared to the simulation; results from a narrow $E_{\mathrm{sum}} = = 18$ MeV region are shown in Figure 1a. The simulation includes boson decay pairs for different boson masses. The disparity parameter y is defined as

$$y = \frac{E_{e^-} - E_{e^+}}{E_{e^-} + E_{e^+}}, \tag{1}$$

where E_{e^-} and E_{e^+} are the kinetic energies of the electron and positron.

Their experimental setup was later upgraded (details?) and used for new measurements. In 2022 the ^{8}Be anomaly was also measured using the $E_p = 441$ keV resonance to produce the 17.64 MeV excited state ($J^\pi = 1^+$, $T = 1$) which again decays primarily to the ground state and the 3.03 MeV state [6]. The anomaly was also measured for $E_p = 650$ and 800 keV where E1 transitions from the direct proton capture dominate [7]. The results for e^+e^- with $E_{\mathrm{sum}} \in [13.5, 20]$ MeV are shown in Figure 1b.

The newer setup was also used in 2021 to study the $^{3}\mathrm{H}(p, e^{+}e^{-})^{4}\mathrm{He}$ reaction at $E_p = 510$, 610 and 900 keV [8], inducing direct and resonant capture populating the overlapping first 20.21 MeV ($J^{\pi} = 0^{+}$) and second 21.01 MeV ($J^{\pi} = 0^{-}$) excited states [9]. The comparison of simulated and measured $e^{+}e^{-}$ pair angular correlations in the $E_{\mathrm{sum}} \in [18, 22]$ MeV region is shown in Figure 1c.

In 2022, another anomaly was measured in the $^{11}\mathrm{B}(p, e^{+}e^{-})^{12}\mathrm{C}$ process [10]. The $E_p = 1388$ keV resonance was used to populate the 17.23 MeV excited state ($J^{\pi} = 1^{-}$, $T = 1$) with a large width $\Gamma = 1.15$ MeV [11]. This state decays mainly through E1 transitions to the ground state $J^{\pi} = 0^{+}$ and to the 4.44 MeV state $J^{\pi} = 2^{+}$. To compensate for energy losses in the target, five energies in the range $E_p = 1.5$–2.5 MeV were used. The experimental angular correlation for the 17.23 MeV transition to the ground state is shown in Figure 1d.

0.1.2 Possible Explanations

0.1.3 Other Experiments

0.2 X17 Project at IEAP CTU

Short summary of our goals, maybe mention the grant.

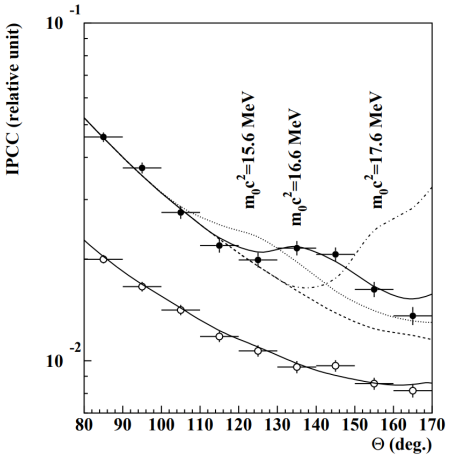

(a) Experimental e^+e^- pair correlations measured in the ^{7}Li$(p, e^+e^-)^8$Be reaction with $|y| \leq 0.5$ (closed circles) and $|y| \geq 0.5$ (open circles) [5].

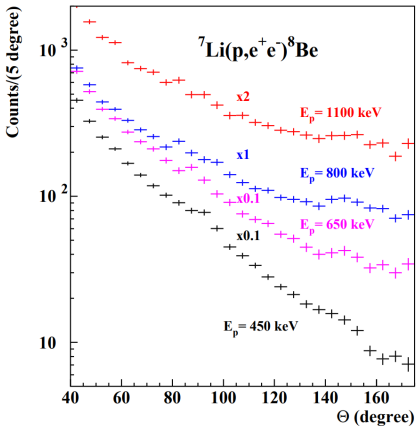

(b) Experimental e^+e^- pair correlations measured in the ^{7}Li$(p, e^+e^-)^8$Be reaction with the improved setup for different proton beam energies [7].

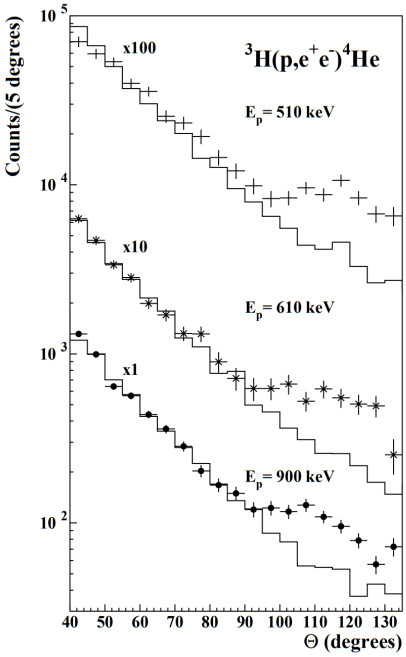

(c) Experimental e^+e^- pair correlations measured in the ^{3}H$(p, e^+e^-)^4$He reaction with $|y| \leq 0.3$ for different proton beam energies [8].

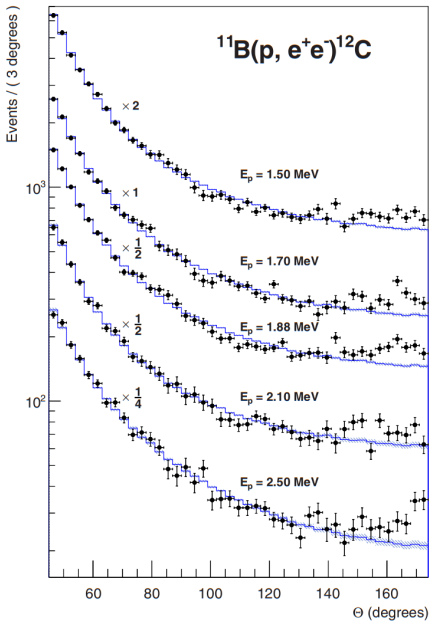

(d) Experimental e^+e^- pair correlations measured in the ^{11}B$(p, e^+e^-)^{12}$C reaction for different proton beam energies [10].

Figure 1: The ATOMKI anomalous IPC measured for different reactions.

1. Time Projection Chamber

Description of TPC, working principle, standard vs. our field layout.

1.1 Orthogonal Fields TPC at IEAP CTU

Short description of our detector. Why we use an atypic TPC (benefits, complications). Gas mixture used in the detector (70/30) and its effect.

1.1.1 Coordinate Systems

In order to describe events in our detector, we use three distinct spaces: the detector space $\mathcal{D}$, the readout space $\mathcal{R}$ and the pad space $\mathcal{P}$. Each space is later used to represent ionization electrons at different stages of the detection process: their creation in the gas, their final position when hitting the readout plane, and finally their representation in the discrete pad space.

Detector Space

The detector space $\mathcal{D}$ represents the physical space of our detector. We describe it using Cartesian coordinates (x, y, z). The z-axis is the detector's axis of symmetry, with its negative direction aligned with the proton beam. The origin $(0, 0, 0)$ is located at the center of the irradiated target. The positive x-axis passes through the center of one the OFTPCs along the intersection of its two planes of symmetry. The y-axis is then chosen to maintain a right-handed coordinate system.

Since the detector has a hexagonal symmetry, we use only one of its sectors in this work – the first sector $\mathcal{D}_1 \subset \mathcal{D}$ which is defined by the condition:

$$(x, y, z) \in \mathcal{D}_1 \Leftrightarrow |y| \leq x \tan \frac{\pi}{6}. \tag{1.1}$$

Simulations in this sector can be applied to all sectors by rotating the coordinates accordingly. The volume of the OFTPC in this sector, which has the shape of a trapezoidal prism, has these boundaries:

$$x \in [x_{\min}, x_{\max}] = [6.51, 14.61] \text{ cm}, \tag{1.2}$$
$$z \in [z_{\min}, z_{\max}] = [-8, 8] \text{ cm}, \tag{1.3}$$
$$y_{\max}(x_{\min}) = -y_{\min}(x_{\min}) = 2.75 \text{ cm}, \tag{1.4}$$
$$y_{\max}(x_{\max}) = -y_{\min}(x_{\max}) = 7.45 \text{ cm}, \tag{1.5}$$

where $y_{\max}(x)$ is the maximal value of the y-coordinate for a given x. The readout is located at $z = 8$ cm; for some purposes, we also define the distance to the readout $d_r = 8 \text{ cm} - z$ as an alternative to the z-coordinate. Keeping this paragraph as it is because the OFTPC volume is distinct from the first sector and some parts of this thesis use the space beyond this volume.

Readout Space

The readout space $\mathcal{R}$ represents the drift time and final positions of ionization electrons as measured by an ideal continuous readout. We describe it using coordinates (x', y', t), where x' and y' correspond to the detector coordinates at the readout plane ($z = 8$ cm). Currently not entirely sure how to put this into a figure since only x' and y' correspond to the detector coordinates. The drift time t is approximately proportional to d_r.

Pad Space

The pad space $\mathcal{P}$ represents the time bin and pad number of ionization electrons as measured by an ideal discrete readout. It is not really a subspace of $\mathcal{R}$ but there is a mapping from $\mathcal{R}$ to $\mathcal{P}$. It is a discretization of a part of $\mathcal{R}$, the mapping can be adjusted depending on the simulation. If we assume uniform electric field there will be gaps, we don't use gaps in the reconstruction since the electrons should be pulled towards the pads.

The readout of the OFTPC will consist (is the design final?) of 128 rectangular pads arranged in a staggered pattern (add image where all the parameters are marked). Most of the pads are 0.6×0.9 cm, only pads 102 and 124 are 0.6×0.6 cm, pad 127 is 0.6×0.509 cm. The distance of neighboring pads is 0.08 cm, staggering offset is 0.3946 cm.

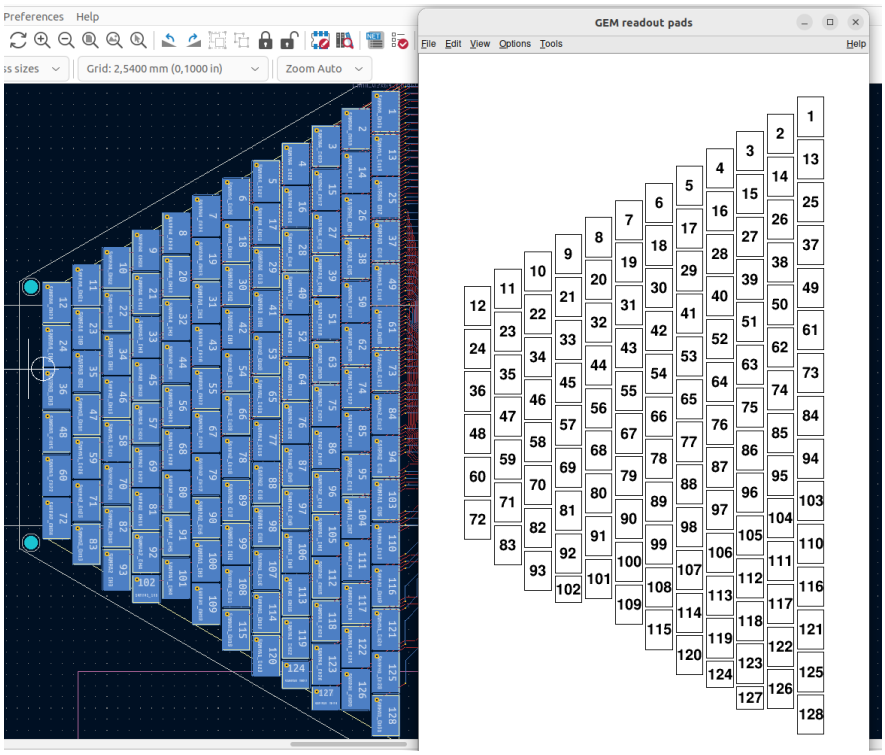

Figure 1.1: Pad layout of the TPC. Swap for better image.

1.1.2 Magnetic Field Simulation

Magnetic field simulations in Maxwell (citation). Some figures. When working with the magnetic field outside the regular grid, we use trilinear interpolation.

Trilinear Interpolation

Trilinear interpolation is a 3D generalization of linear interpolation. It can be used to interpolate a function whose values are known on a regular grid with rectangular prism cells. We use this simple method for interpolating the magnetic field, and it is later used in Section 3.2.1 to interpolate the Ionization Electron Map, a key component of our track reconstruction algorithm. In both cases, we use a regular cubic grid (apparently it is also called a Cartesian grid).

Could put a paragraph about linear interpolation here if it is not clear from the equations below.

Let us consider a cell of our regular grid (a cube) with an edge of length a containing the point $\mathbf{C} = (x, y, z)$ where we want to interpolate a function $f\colon \mathbb{R}^3 \to \mathbb{R}$. We know the values of this function at the vertices of the cell $\mathbf{C}_{ijk} = (x_0 + ia, y_0 + ja, z_0 + ka)$, where $i, j, k \in \{0, 1\}$ are indices. We also define the points $\mathbf{C}_{ij} = (x, y_0+ia, z_0+ja)$ and $\mathbf{C}_i = (x, y, z_0+ia)$. Then the interpolated value $\widehat{f}(\mathbf{C})$ can be calculated as a composition of three linear interpolations (see Figure 1.2):

$$\widehat{f}(\mathbf{C}_{ij}) = (1 - x_d)\, f(\mathbf{C}_{0ij}) + x_d\, f(\mathbf{C}_{1ij}), \tag{1.6}$$

$$\widehat{f}(\mathbf{C}_i) = (1 - y_d)\, \widehat{f}(\mathbf{C}_{0i}) \;\; + y_d\, \widehat{f}(\mathbf{C}_{1i}), \tag{1.7}$$

$$\widehat{f}(\mathbf{C}) = (1 - z_d)\, \widehat{f}(\mathbf{C}_0) \;\; + z_d\, \widehat{f}(\mathbf{C}_1), \tag{1.8}$$

where x_d, y_d, and z_d are given as follows:

$$x_d = \frac{x - x_0}{a},\;\; y_d = \frac{y - y_0}{a},\;\; z_d = \frac{z - z_0}{a}. \tag{1.9}$$

We can also write

$$\widehat{f}(\mathbf{C}) = \sum_{i,j,k \in \{0,1\}} t_x^i t_y^j t_z^k f(\mathbf{C}_{ijk}), \tag{1.10}$$

$$t_\alpha \overset{\text{def}}{=} \begin{pmatrix} t_\alpha^0 \\ t_\alpha^1 \end{pmatrix} = \begin{pmatrix} 1 - \alpha_d \\ \alpha_d \end{pmatrix}, \tag{1.11}$$

where $\alpha \in \{x, y, z\}$ is an index. Furthermore, we can write $\widehat{f}(\mathbf{C})$ as a polynomial:

$$\widehat{f}(\mathbf{C}) = \sum_{\alpha,\beta,\gamma \in \{0,1\}} \sum_{i=0}^{\alpha} \sum_{j=0}^{\beta} \sum_{k=0}^{\gamma} (-1)^{(\alpha-i)+(\beta-j)+(\gamma-k)} f(\mathbf{C}_{ijk}) x_d^\alpha y_d^\beta z_d^\gamma. \tag{1.12}$$

We take advantage of this form when generalizing trilinear interpolation to irregular grid in section 3.2.2.

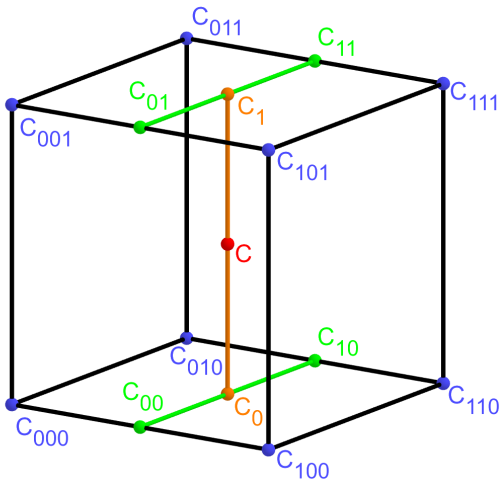

Figure 1.2: Visualization of trilinear interpolation as a composition of linear interpolations. Image drawn in GeoGebra and inspired by a similar image on Wikipedia (which looks a bit worse) – is credit necessary?

Maybe a citation here, although I am not sure it is necessary since it could be considered common knowledge. The last two equations are my own. Maybe x_0, etc. should be explicitly described.

2. Track Simulation

In order to develop and test the reconstruction algorithm, electron and positron tracks are simulated inside the first sector $\mathcal{D}_1$ of our detector (see Section 1.1.1) with different initial parameters. Two approaches are currently used to simulate tracks, each of them for different purpose.

The **Microscopic Simulation** uses the Garfield++ toolkit [1]. Within this toolkit, the High Energy Electro-Dynamics (HEED) program [13] is used to simulate the primary particle and the class *AvalancheMicroscopic* to simulate the drift of secondary electrons created by ionization in the gas. This is the most precise and time-consuming simulation used; our current goal is to be able to successfully reconstruct its results and determine our best-case energy resolution.

The **Runge-Kutta Simulation** uses the 4th order Runge-Kutta numerical integration (add citation for Runge-Kutta) to simulate the trajectory of the primary particle in the electromagnetic field inside the detector. It is relatively fast since it does not simulate the secondary particles. It is used as part of our reconstruction algorithm and for testing some parts of the reconstruction.

All of these simulations require the knowledge of the electromagnetic field inside the detector. A uniform electric field of 400 $\mathrm{V{\cdot}cm^{-1}}$ is assumed. The magnetic field was simulated in Maxwell (see Section 1.1.2). add citation

Single track in positive x direction or initial parameter randomization. Importance of gas composition, used gas compositions.

2.1 Microscopic Simulation

The microscopic simulation, the most detailed simulation used in this work, is performed using the Garfield++ toolkit [1].

The electron transport properties are simulated using the program Magboltz (Add citation.). Two different gas mixtures were used: 90% Ar + 10% CO_2 and 70% Ar + 30% CO_2. The second mixture will be used in our detector. The temperature is set to 20 °C, the pressure is atmospheric.

The primary track is simulated using the program HEED [13], which is an implementation of the photo-absorption ionization model. This program provides the parameters of ionizing collisions. HEED can also be used to simulate the transport of delta electrons; we do not account for these in the current simulation but plan to include them in the future. The photons created in the atomic relaxation cascade (fluorescence reabsorption, ?) are also not simulated.

Finally, we use the microscopic tracking provided by the class *AvalancheMicroscopic* to simulate the drift of the ionization electrons. Each electron is followed from collision to collision using the equation of motion and the collision rates calculated by Magboltz.

First simulated track in the z direction should be described in detail here (own subsection?). Figures.

Add more detailed and better description of HEED, and microscopic tracking (each their own subsection?). Could also mention Monte Carlo (requires gas file generation) and Runge-Kutta simulation implemented in Garfield, why we don't

use them (another subsection? rename the section to Garfield++ simulation and mention all relevant parts?).

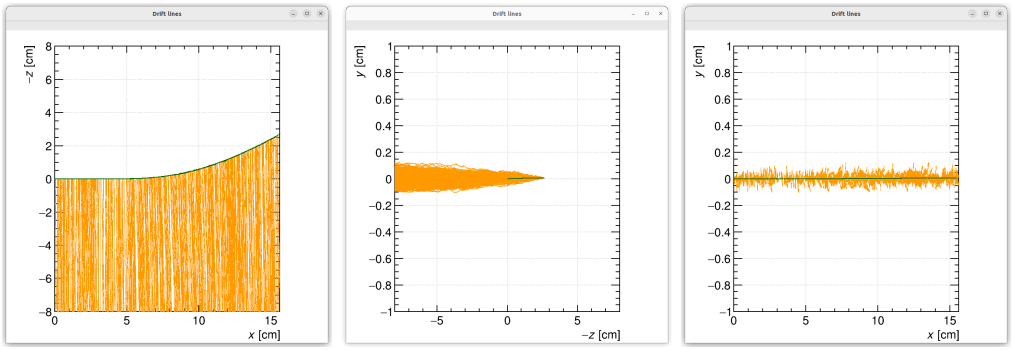

Figure 2.1: Example of a simulated electron track in 70 % argon and 30 % CO_2 atmosphere (on the left). Swap for better images, better zoom. Explain drift lines, primary particle.

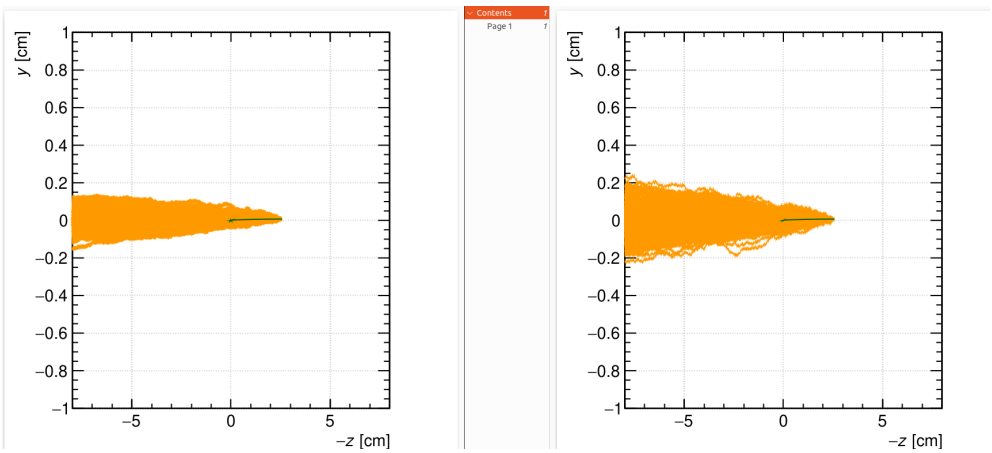

Figure 2.2: Comparison of diffusion in a simulated electron track in 70 % argon, 30 % CO_2 atmosphere and in 90 % argon, 10 % CO_2 atmosphere (on the right). Swap for better image, better zoom. Or put the same pictures for both comparisons in one subfigure, etc. Describe better.

2.2 Runge-Kutta Simulation

Trajectory simulation with 4th order Runge-Kutta. Relativistic equation that is numerically integrated by the algorithm.

3. Track Reconstruction

In the first stage of the reconstruction algorithm, we reconstruct the track of a primary particle (either an electron or a positron). The result of this step is then used to determine the energy of the particle (Section 4).

The **Reconstruction Assuming Steady Drift** uses the standard TPC approach. With parallel fields, the drift inside a uniform electric field remains undistorted (reference to some future part of the TPC chapter). Therefore, we only need to reconstruct the z-coordinate from the drift time using the known drift velocity. We also assume that the readout coordinates (x', y', t) are known exactly, neglecting the pads and time bins.

Reconstruction using the **Ionization Electron Map** (from now on referred to as *the map*) uses a simulation of the drift of secondary (ionization) electrons within the detector volume. This simulation can then be used to interpolate the initial position of the secondary electrons. First attempts neglect the pads.

We use the map for reconstruction in two different ways. The first one uses gradient descent search along with trilinear interpolation (see Section 1.1.2) of the map. The second method uses interpolation on the irregular inverse grid with a linear polynomial.

The **Discrete Reconstruction** uses the map; instead of reconstructing the exact position of each electron, we reconstruct the center of each hit pad with the time corresponding to the midpoint of the time bin. The electron count in each TPC bin (consisting of the pad and the time bin) serves as the charge value, which is then used as a weight in the energy reconstruction fit.

3.1 Reconstruction Assuming Steady Drift

As the first step, we decided to try to reconstruct an electron track with a special set of initial parameters. The origin of the particle is given by the origin of our coordinate system. The initial direction is given by the positive x-axis. This means the magnetic field of our detector is perpendicular to the momentum of the particle at all times, and we can reduce the problem to two-dimensional space. As an example. we use a track simulated using the microscopic simulation (see Section 2.1) with a kinetic energy of 8 MeV. The gas composition used in this simulation is 90% Ar + 10% CO_2. Might be better to describe this track in Section 2.1.

In this approach to the reconstruction of the track, we decided to use the common method used in a standard TPC. This will allow us to explore the significance of the atypical behavior in our OFTPC. Additionally, we assume the readout is continuous to further simplify the problem. In this approximation, we reconstruct the initial position of each ionization electron.

The reconstruction is then defined by the following relations between the coordinates of the detector space and the readout space (see Section 1.1.1):

$$x = x', \tag{3.1}$$
$$y = y', \tag{3.2}$$
$$z = v_d t, \tag{3.3}$$

where v_d is the drift velocity of electrons in the given gas mixture. At a phenomenological level, this velocity can be considered as a function of the electric field $\boldsymbol{E}$ and the magnetic field $\boldsymbol{B}$:

$$v_d = v_d(\boldsymbol{E}, \boldsymbol{B}). \tag{3.4}$$

Equation taken from Garfield user manual. The Garfield++ toolkit uses this fact to accelerate their drift simulation with non-microscopic approaches (could mention in the simulation chapter). Since we assume a uniform electric field in our detector and we want to neglect the effect of our unusual magnetic field, we consider the drift velocity to be constant in this scenario. We then approximate this velocity by fitting the dependence $z(t)$ taken from the simulated ionization electrons. This is in one of the provisional figures. Also, this description is not completely accurate; in reality, we fit t1:8-y0 with a1*x+a0 and then invert this and use 8-y0 = b1*t1+b0 (old coordinates); b1=1/a1 functions as the drift velocity. Maybe also define this 8-z variable as an alternative to z in Section 1.1.1 and then use it when correcting this.

Later, in a commit after this, I plotted some residues (provisional figure), which could be useful, but for some reason they are residuals from a spline fit of the track?! Probably redo this without the spline fit; just explore the difference in individual points.

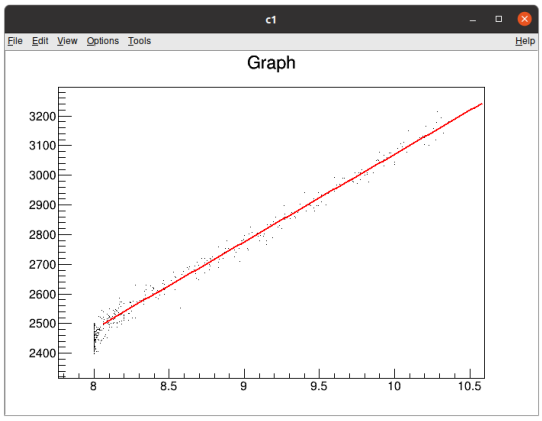

Figure 3.1: Dependence of the drift time on the z coordinate in 90 % argon and 10 % CO_2 atmosphere, fitted with a linear function. The fitted function gives us the average drift velocity in the gas and can be used for rough reconstruction in our TPC. Swap for better image with axis labels, etc. Maybe write the fitted equation.

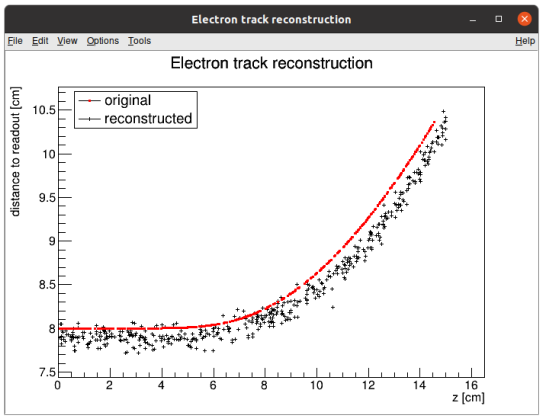

Figure 3.2: First attempt at a track reconstruction using only the drift velocity. This approach works well in a standard TPC (ideally cite some source?). 90 % argon and 10 % CO_2 atmosphere. Swap for better image, correct coordinates.

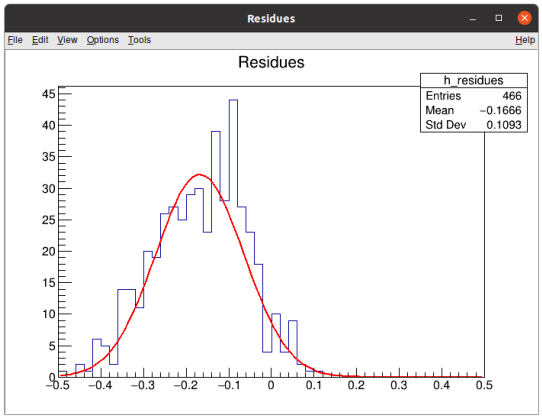

Figure 3.3: First attempt at a track reconstruction using only the drift velocity, residues. Swap for better image, correct coordinates. What's causing the shift? Explain details.

3.2 Ionization Electron Map

Inside an OFTPC, the drift of the secondary (ionization) electrons is significantly affected by its magnetic field (pictures of the distortion later, the effect is bigger for the 90/10 composition.). We need to take this into account for accurate reconstruction. In the first approximation, we assume a continuous readout (i.e., we neglect pads). We can then reconstruct the original position of each ionization electron using its readout coordinates. For this purpose, we use the ionization electron map.

The ionization electron map represents a mapping from the detector space to the readout space (see Section 1.1.1). It tells us what readout coordinates (x', y', t) we can expect on average for an ionization electron created at the detector coordinates (x, y, z). More precisely it is a mapping to the distributions on the readout space; we can simplify this as only the means $\overline{\mathcal{M}}$ and the covariance

matrices $\mathcal{M}_{\text{cov}}$, assuming Gaussian distribution.

$$\mathcal{M} : \mathcal{D} \longrightarrow \mathcal{R},\ (x, y, z) \longmapsto (x', y', t). \tag{3.5}$$

To get an approximation of this mapping, we simulate the drift of ionization electrons generated on a regular grid inside the volume of our OFTPC [1]. It is also useful to simulate multiple (100 in our case) electrons originating from the same position so we can get a better information about the average drift and its variance. In order to get more accurate results, we use the microscopic simulation of these electrons described in Section 2.1. When evaluating the map inside the grid, we use trilinear interpolation (see Section 1.1.2). From now on, we will denote this interpolated simulation with the same symbol $\mathcal{M}$.

Finally, we need to invert the map to get the original detector coordinates (x, y, z) for the given readout coordinates (x', y', t). In our case, we can reasonably assume that the mapping $\overline{\mathcal{M}}$ is one-to-one (as seen in the simulations). We implemented two methods for this purpose: the gradient descent search (Section 3.2.1) and interpolation on the inverse grid (Section 3.2.2).

The simulation of the map is a computationally heavy task. For this reason, we use the MetaCentrum grid [3] to parallelize needed calculations. At first, this was done by evenly distributing the simulated electrons across the individual jobs in a simulation with only one electron per vertex in the regular grid with a spacing of one centimeter.

Later, a more efficient approach was implemented, accounting for the varying lengths of the drift of individual electrons. If we index the electrons in the order of increasing coordinates y, x, z (picture?), we can express the number n_l of full XY layers (i.e., electrons with the same z coordinate) of electrons with index less than or equal to i

$$n_l(i) = \left\lfloor \frac{i}{n_{xy}} \right\rfloor, \tag{3.6}$$

where n_{xy} is the number of electrons in each XY layer calculated simply by counting the electrons that satisfy boundary conditions for x and y. These conditions should be mentioned above; sector condition + maximal x value. The number of electrons remaining in the top layer is then

$$n_r(i) = i \bmod n_{xy}. \tag{3.7}$$

Finally, we can calculate the sum of the drift gaps of electrons up to index i

$$d_{\text{sum}} = (z_{\max} - z_{\min}) n_{xy} n_l - \frac{n_l(n_l - 1)}{2} n_{xy} l + n_r(z_{\max} - z_{\min} - n_l l). \tag{3.8}$$

We then use a binary search algorithm to find the maximum index i such that the value of this sum is less than the fraction $\frac{\text{job id}}{\text{max job id}}$ of the total sum. This way we obtain the minimal and the maximal index of electrons simulated in the given job. The spacing l should be probably defined above + picture of the simulating grid (1 layer). zmin zmax also

After the simulation of the map, we calculate the mean readout coordinates assuming Gaussian distribution (i.e., we use averages). We also calculate standard

[1] we do not take the detector walls into account and simulate even outside of the OFTPC which lets us interpolate even close to the walls

deviations in a later commit, should be upgraded to the covariance matrix. We never actually plotted the distributions we get when simulating the same electron multiple times, so we do not know if our assumptions are accurate (could also run some statistical test to see how well the Gaussian distribution fits).

The obtained map is then stored in a custom class template *Field*, could expand on that. Maybe earlier, since the same template is used for the magnetic field.

Could insert a table here describing all 4 simulations of the map (gas composition, spacing, etc.). Simulation inside of one sector (at first double angle). Extra space on the sensor. Edge cases not taken into account (TPC wall). Using qsub (not sure if important). Add plots of distortion of the coordinates. Could also do these plots in a different way (e.g., drawing all the endpoints of each ionization electron or some error ellipse plot).

Images to add (comparison of both simulations):

- 3D visualization of the map, simulation example
- z vs. t plot
- XY plane distortion for different z values; with arrows and error bars, for all z-layers with different colors
- XZ plane ($y = 0$) distortion in x (maybe not necessary?)
- XT plot ($y = 0$) showing (small) distortion in drift times

More images:

- Residuals of the continuous readout reconstruction.

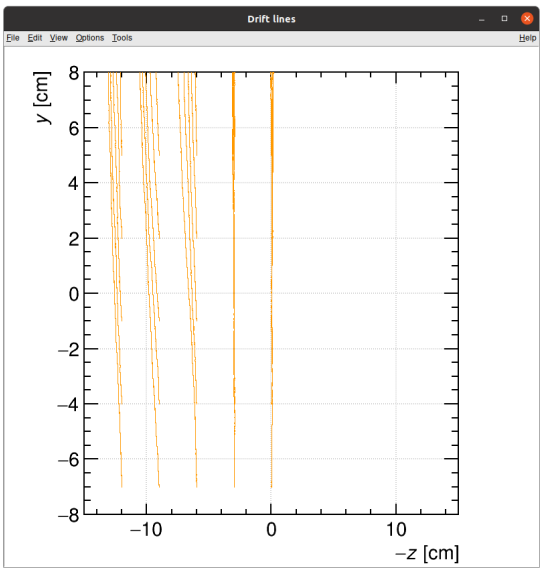

Figure 3.4: Example of map generation. Swap for better image, correct coordinates.

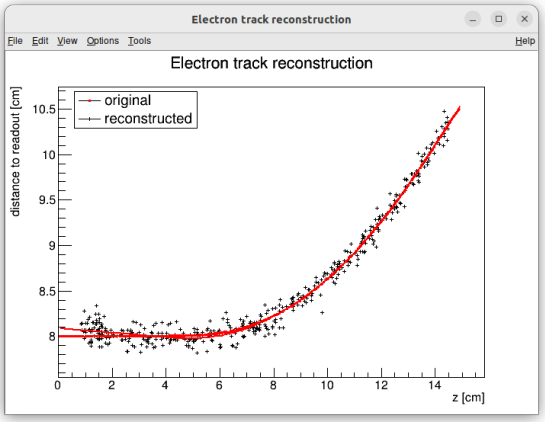

Figure 3.5: Example reconstruction with the map. Swap for better image, correct coordinates.

3.2.1 Gradient Descent Search

The first implemented method of reconstruction uses a gradient descent search to calculate an inversion of the map $\overline{\mathcal{M}}$ in a given point. Gradient descent is an iterative minimization algorithm for multivariate functions. Let $R \in \mathcal{R}$ be a point in the readout space; we want to find a point $D = (x, y, z) \in \mathcal{D}$ in the detector space such that

$$\overline{\mathcal{M}}(D) = R = (x'_R, y'_R, t_R). \tag{3.9}$$

We define a function f_R in the readout space as a distance in this space:

$$f_R(x', y', t) = \sqrt{(x' - x'_R)^2 + (y' - y'_R)^2 + v_d^2(t - t_R)^2}, \tag{3.10}$$

where v_d is an approximation of the drift velocity in the TPC, obtained from the reconstruction in Section 3.1 (there will be an image with the linear fit there). We make an initial guess (actually in the original code we just take $z = 0$):

$$D_0 = (x'_R, y'_R, v_d t). \tag{3.11}$$

Assuming we have the n-th estimate D_n, we calculate the i-th component of the gradient of $f_R \circ \overline{\mathcal{M}}$ numerically using central differences:

$$\left[\nabla(f_R \circ \overline{\mathcal{M}})\right]^i (D_n) \approx \frac{f_R(\overline{\mathcal{M}}(D_n + s \cdot e^i)) - f_R(\overline{\mathcal{M}}(D_n - s \cdot e^i))}{2s}, \tag{3.12}$$

where $e^i \in \mathcal{D}$ is the i-th coordinate vector and s is the step size. The step size should be sufficiently small; initially, we set it as a fraction of the map's grid spacing $s = \frac{l}{10}$. During the minimization, we check that $f_R(\overline{\mathcal{M}}(D_n)) < 10s$ at all times. When using trilinear interpolation, it would be more efficient to calculate the gradient explicitly (± same result). This could be implemented inside the *Field* template class. The next iteration can be calculated as follows:

$$D_{n+1} = D_n - \gamma \nabla(f_R \circ \overline{\mathcal{M}})(D_n), \tag{3.13}$$

where $\gamma \in \mathbb{R}^+$ is the damping coefficient. It should be set to a small enough value to ensure convergence, but large enough for sufficient converging speed.

The minimization stops either when the error $f_R(\overline{\mathcal{M}}(D_n))$ drops below a specified value or when the number of iterations exceeds a certain limit (in this case, a message is printed into the console). The parameters of this method can be further optimized (e.g., a better choice of γ, gradient computation); instead, we later decided to use the interpolation on the inverse grid described in the next section.

Measure reconstruction duration and compare it with the inverse grid interpolation? Also compare the result? Not sure if this has to be cited.

3.2.2 Interpolation on the Inverse Grid

Interpolating between known points in the readout space. Gaussian elimination, multivariate polynomial. Benefits compared to the gradient descent search method (one-time computation for the whole map is easy to achieve if needed).

The currently used baseline reconstruction method is the interpolation on the inverse grid. Rather than attempting to invert the trilinearly interpolated map as in the previous section, we take advantage of the fact that the map $\overline{\mathcal{M}}$ is one-to-one (isomorphism is supposed to preserve structure, not sure how to interpret that here). Since we have simulated values of this map on a regular grid in the detector space $\mathcal{D}$, we also know the inverse map $\overline{\mathcal{M}}^{-1}$ on the irregular inverse grid in the readout space $\mathcal{R}$. To get an approximation of the inverse map in the entire readout space, we can use interpolation.

Since the inverse grid is irregular, trilinear interpolation cannot be applied. Given that the simulated map is dense enough to provide a good approximation considering the size of our pads, we can adopt a similar approach (more complicated and computationally heavy alternative would be natural neighbor interpolation). As shown in Equation 1.12 in Section 1.1.2, trilinear interpolation can be expressed as a polynomial:

$$\widehat{f}(x, y, z) = axyz + bxy + cxz + dyz + ex + fy + gz + h, \tag{3.14}$$

where a, b, c, d, e, f, g, h are coefficients uniquely determined by the values of the function at the vertices of the interpolation cell. We can generalize this for a function defined on an irregular grid. Given the function values at any eight points, we can write a system of eight linear equations

$$\begin{pmatrix} x_1y_1z_1 & x_1y_1 & x_1z_1 & y_1z_1 & x_1 & y_1 & z_1 & 1 \\ \vdots & \vdots & \vdots & \vdots & \vdots & \vdots & \vdots & \vdots \\ x_8y_8z_8 & x_8y_8 & x_8z_8 & y_8z_8 & x_8 & y_8 & z_8 & 1 \end{pmatrix} \begin{pmatrix} a \\ \vdots \\ h \end{pmatrix} = \begin{pmatrix} f(x_1, y_1, z_1) \\ \vdots \\ f(x_8, y_8, z_8) \end{pmatrix}, \tag{3.15}$$

which has a unique solution for the coefficients for most values of (x_n, y_n, z_n) and $f(x_n, y_n, z_n)$, where $n \in \{1, \ldots, 8\}$.

This approach introduces a small complication: finding the correct pseudocell (i.e., the image of eight vertices forming a cubic cell in the regular grid) in the inverse grid. The eight irregularly spaced vertices of this pseudocell do not define a unique volume, so there are multiple possible ways to partition $\mathcal{R}$ into pseudocells, with no obvious choice among them.

We are currently ignoring this problem and performing binary search along x, y, z (in this order). It shouldn't matter too much because the 70/30 map

doesn't cause such a big distortion and was even accidentally extrapolated for all z different from the central plane. Interpolation should be generally faster than the gradient descent since we don't need to iterate. We also don't need to optimize it to improve performance, if it's too slow we can even calculate the coefficients for the entire map before reconstruction.

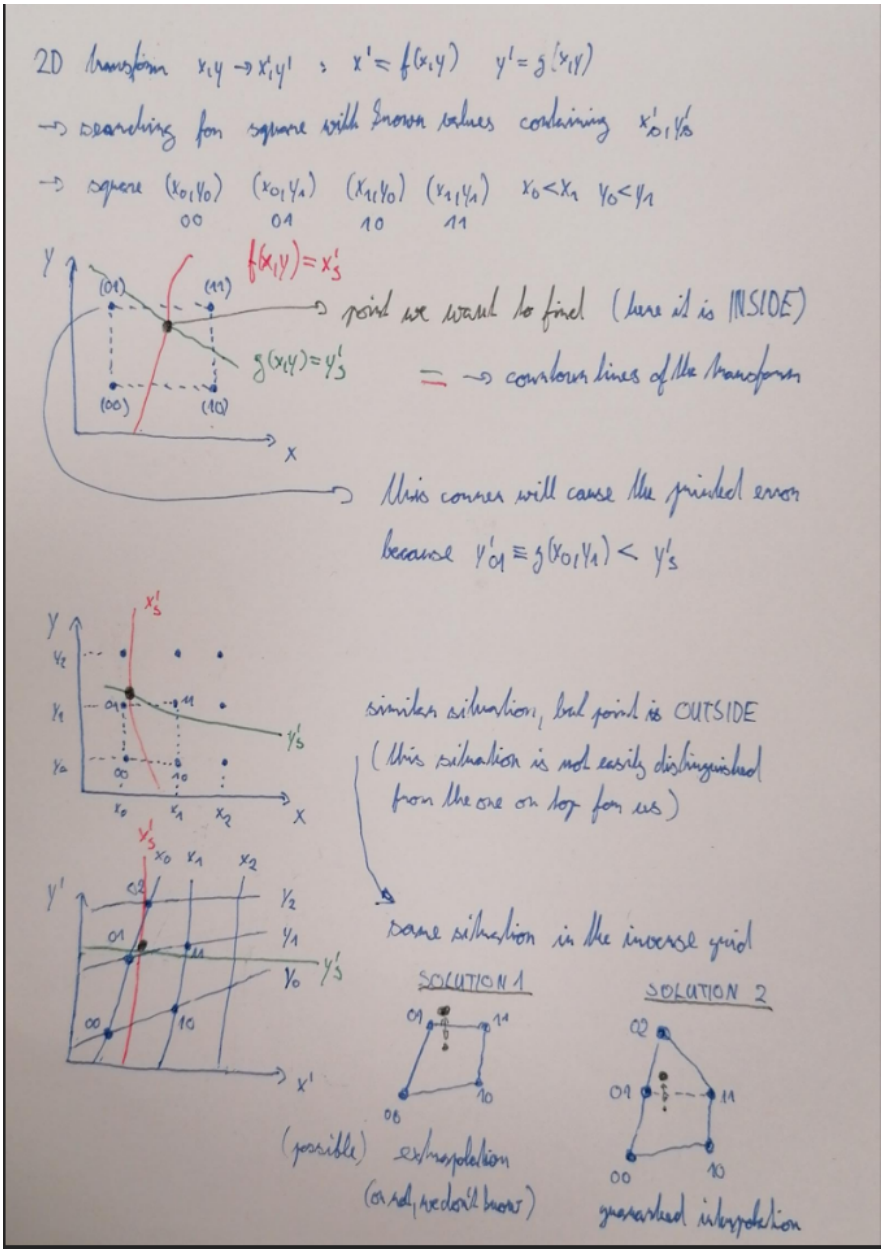

Figure 3.6: Selection of the points for interpolation. Create better images; use the explanation interpolation vs. extrapolation strange property. Solution 2 probably does not make much sense.

3.3 Discrete Reconstruction

Reconstruction with pads and time bins. Maybe testing different pads. Mapping the center of the pad (along with the midpoint of the time bin) isn't necessarily

the best approach since it might not correspond to the average parameters of an electron with these readout parameters (insignificant?).

It is also possible to make this a subsection of the map, making the previous subsections parts of a new subsection 'Map Inversion'.

4. Energy Reconstruction

The second stage is the reconstruction of the particle's energy using a fit of its reconstructed track (see Section 3). We have tested three ways of reconstructing the energy. Fitting is done using the MINUIT algorithm implemented in ROOT [2]. Cite some CERN article directly on MINUIT, can add a section.

The **Cubic Spline Fit** is a tested and later rejected method of energy reconstruction. It uses smoothly connected piecewise cubic polynomials between uniformly spaced nodes. Energy is calculated using the fit parameters by computing the radius of curvature in different points of the fitted curve using the known magnitude of the magnetic field perpendicular to the trajectory. We rejected this method because tuning of the fit to have a reasonably stable radius of curvature turned out to be unpractical.

The **Circle and Lines Fit** was chosen as an alternative since this corresponds to the shape of a trajectory of a charged particle crossing a finite volume with a homogeneous magnetic field. The energy of the particle can be estimated using the fitted radius and the magnitude of the perpendicular magnetic field in the middle of the TPC.

The **Runge-Kutta Fit** uses the 4th order Runge-Kutta numerical integration described in Section 2.2. Initial parameters of the track (including the particle's energy) are optimized so that the integrated trajectory fits to the reconstructed one. This fit can also be performed as a single parameter (i.e., energy) fit if we get the initial position and orientation of the particle on the entrance to the TPC from previous detectors (Timepix 3 (Tpx3) and Multi-Wire Proportional Chamber (MWPC), see Section 0.2).

4.1 Cubic Spline Fit

The first attempt to get an early estimate of the kinetic energy of the particle uses a cubic spline fit. We use an electron track starting in the origin of our coordinate system with an initial direction in the positive x axis. The example track is simulated microscopically (see Section 2.1) with a kinetic energy of 8 MeV in a gas mixture 90% Ar + 10% CO_2 (the same track was used in Section 3.1).

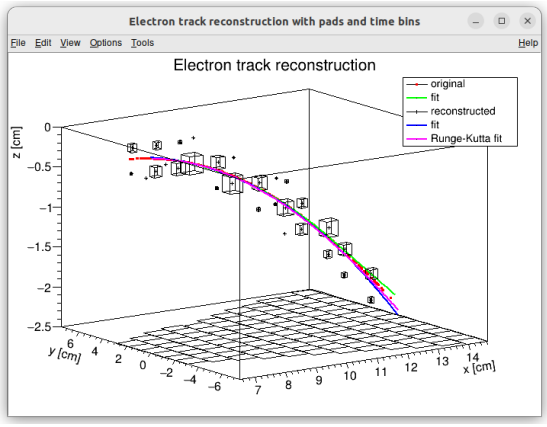

Figure 4.1: Example of a fitted reconstructed track. Swap for better image.

This track should probably be described in the simulation chapter.

In order to calculate the spline, we use the class *TSpline3* from ROOT. This allows us to evaluate the spline using the coordinates (x_n, z_n) of each node and the derivatives d_1, d_2 in the first and the last node. We can fit these parameters of a fixed amount of nodes to the simulated trajectory. We use the IMPROVE algorithm provided by the *TMinuit* class in ROOT. This algorithm attempts to find a better local minimum after converging.

After the fit, we want to get an energy estimate. In order to calculate it, we need the radius of curvature, which we get from the fitted spline at every point of the trajectory. The part of the spline corresponding to a given node is defined as

$$z(x) = z_n + b\Delta x + c(\Delta x)^2 + d(\Delta x)^3, \tag{4.1}$$

where $\Delta x = x - x_n$ and b, c, d are coefficients. Using this equation, we derive the radius of curvature[1] as:

$$r(x) = \frac{(1 + z'^2(x))^{\frac{3}{2}}}{z''(x)} = \frac{\left(1 + (b + 2c\Delta x + 3d(\Delta x)^2)^2\right)^{\frac{3}{2}}}{2c + 6d\Delta x}. \tag{4.2}$$

Based on the geometry of the detector, we can assume the magnetic field $\boldsymbol{B}(x, 0, z) = (0, B(x, z), 0)$ for a track in the XZ plane. Since the electron is relativistic, the effect of the electric field on its trajectory is negligible. The Lorentz force F_L is then always perpendicular to the momentum of the electron and acts as a centripetal force F_c:

$$\boldsymbol{F_L} = \boldsymbol{F_c}, \tag{4.3}$$

$$\|e\boldsymbol{v} \times \boldsymbol{B}\| = \frac{\gamma m_e v^2}{r}, \tag{4.4}$$

$$ec\beta B = \frac{E_{0e}\beta^2}{r\sqrt{1-\beta^2}}, \tag{4.5}$$

$$\sqrt{1-\beta^2} = \frac{E_{0e}\beta}{ecBr}, \tag{4.6}$$

$$\beta^2(x) = \left[1 + \left(\frac{E_{0e}}{ecB(x, z(x))r(x)}\right)^2\right]^{-1}, \tag{4.7}$$

where e is the elementary charge, c is the speed of light in vacuum, m_e is the rest mass of electron, $E_{0e} = m_e c^2$ is the corresponding energy, γ is the Lorentz factor, $\boldsymbol{v}$ is the velocity of the electron, and $\beta = \frac{v}{c}$. We can then finally get our estimate of the kinetic energy for a given point on the trajectory as follows:

$$E_{\text{kin}}(x) = \left(\frac{1}{\sqrt{1-\beta^2(x)}} - 1\right) E_{0e}. \tag{4.8}$$

We can then average these estimates at multiple points to get one final estimate. This method was later rejected in favor of the circle and lines fit described in Section 4.2. Add some figures.

[1] For the general formula see `https://en.wikipedia.org/wiki/Curvature#Graph_of_a_function`

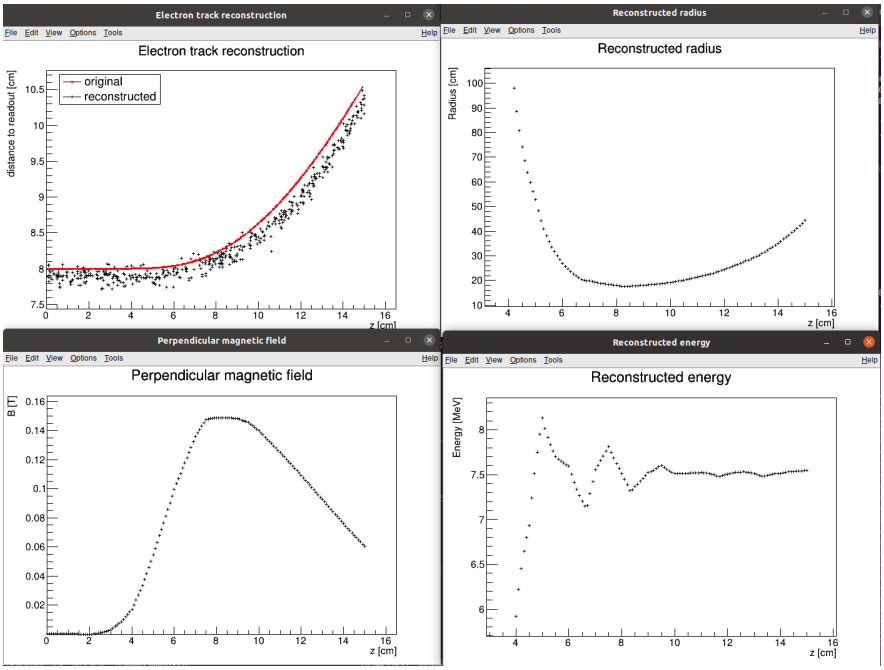

Figure 4.2: First attempt at a track reconstruction using only the drift velocity. Spline energy reconstruction attempt. Swap for better image(s) – subfigure environment, correct coordinates.

4.2 Circle and Lines Fit

Another way to estimate the particle's kinetic energy is to fit its trajectory with a circular arc with lines attached smoothly. This shape of trajectory corresponds to a movement of a charged particle through a homogeneous magnetic field perpendicular to the particle's momentum and limited to a certain volume. In general, the shape of such a trajectory in a non-perpendicularly oriented field is a spiral. In our case, this component is negligible since the field is approximately toroidal and the particle motion is nearly perpendicular to it. At first, we tested a 2D version of this fit, then we adapted it to 3D.

Our field is not homogeneous, it is therefore not entirely clear what value of magnetic field should be used along with the fitted radius (using equations 4.7 and 4.8) to get the best estimate for the kinetic energy. Since we only use this method as the first iteration of the particle's energy that we later refine, an optimal solution of this problem is not required. Instead, we tested two options: taking the value of the field in the middle of the fitted circular arc and taking the average field along it. We haven't really tried to plot this for multiple tracks, but these estimates are saved somewhere and could be plotted.

4.2.1 Two-dimensional fit

In the 2D case, the fitted function used for the electron track[2] described in Section 4.1 is defined as follows: Maybe describe this track that we used at the beginning somewhere earlier (section microscopic simulations → Testing track?) so that it is easier to refer to it in multiple sections. It is not part of the early GitHub

[2]Electron tracks bend towards negative z, we need to use the upper part of the circle

commits, so maybe it won't be possible to create exact replicas of the images, but they should be at least very similar.

$$z(x) = \begin{cases} a_1 x + b_1 & x < x_1 \\ z_0 + \sqrt{r^2 - (x - x_0)^2} & x_1 \leq x \leq x_2 \\ a_2 x + b_2 & x > x_2 \end{cases}, \tag{4.9}$$

where $a_{1,2}$ and $b_{1,2}$ are the parameters of the lines, (x_0, z_0) is the center of the circle, r is its radius, and $(x_{1,2}, z_{1,2})$ are the coordinates of the function's nodes. That means we have 9 parameters ($z_{1,2}$ are not used in the function) along with 2 continuity conditions and 2 smoothness conditions. For the fit, we use the coordinates of the nodes and the radius of the circle, which gives us 5 independent parameters (only the radius has to be larger than half of the distance between nodes). The continuity conditions (combined with the relations for $z_{1,2}$) are as follows:

$$z_{1,2} = a_{1,2} x_{1,2} + b_{1,2} = z_0 - \sqrt{r^2 - (x_{1,2} - x_0)^2}. \tag{4.10}$$

The smoothness conditions are as follows:

$$a_{1,2} = \frac{x_0 - x_{1,2}}{\sqrt{r^2 - (x_{1,2} - x_0)^2}}. \tag{4.11}$$

Equation 4.10 gives us the values of $b_{1,2}$

$$b_{1,2} = z_{1,2} - a_{1,2} x_{1,2}. \tag{4.12}$$

For the coordinates of the center of the circle, we can use the fact that the center has to lie on the axis of its chord. In other words, there is a value of a parameter t such that, using the parametric equation of the axis

$$\begin{pmatrix} x_0 \\ z_0 \end{pmatrix} = \begin{pmatrix} \frac{x_1 + x_2}{2} \\ \frac{z_1 + z_2}{2} \end{pmatrix} + t \begin{pmatrix} \frac{z_2 - z_1}{2} \\ \frac{x_1 - x_2}{2} \end{pmatrix}. \tag{4.13}$$

At the same time, the center has to be in a distance of r from the nodes:

$$(x_1 - x_0)^2 + (z_1 - z_0)^2 = r^2, \tag{4.14}$$

$$\left(\frac{x_1 - x_2}{2} + \frac{z_1 - z_2}{2} t\right)^2 + \left(\frac{z_1 - z_2}{2} + \frac{x_2 - x_1}{2} t\right)^2 = r^2, \tag{4.15}$$

$$\left(\left(\frac{x_2 - x_1}{2}\right)^2 + \left(\frac{z_2 - z_1}{2}\right)^2\right) t^2 + \left(\frac{x_2 - x_1}{2}\right)^2 + \left(\frac{z_2 - z_1}{2}\right)^2 - r^2 = 0. \tag{4.16}$$

Since our electron track bends towards negative z and $x_2 > x_1$, we only care about the solution with $t > 0$

$$t = \sqrt{\frac{r^2}{\left(\frac{x_2 - x_1}{2}\right)^2 + \left(\frac{z_2 - z_1}{2}\right)^2} - 1}, \tag{4.17}$$

$$x_0 = \frac{x_1 + x_2}{2} + \frac{z_2 - z_1}{2} \sqrt{\frac{r^2}{\left(\frac{x_2 - x_1}{2}\right)^2 + \left(\frac{z_2 - z_1}{2}\right)^2} - 1}, \tag{4.18}$$

$$z_0 = \frac{z_1 + z_2}{2} - \frac{x_2 - x_1}{2} \sqrt{\frac{r^2}{\left(\frac{x_2 - x_1}{2}\right)^2 + \left(\frac{z_2 - z_1}{2}\right)^2} - 1}. \tag{4.19}$$

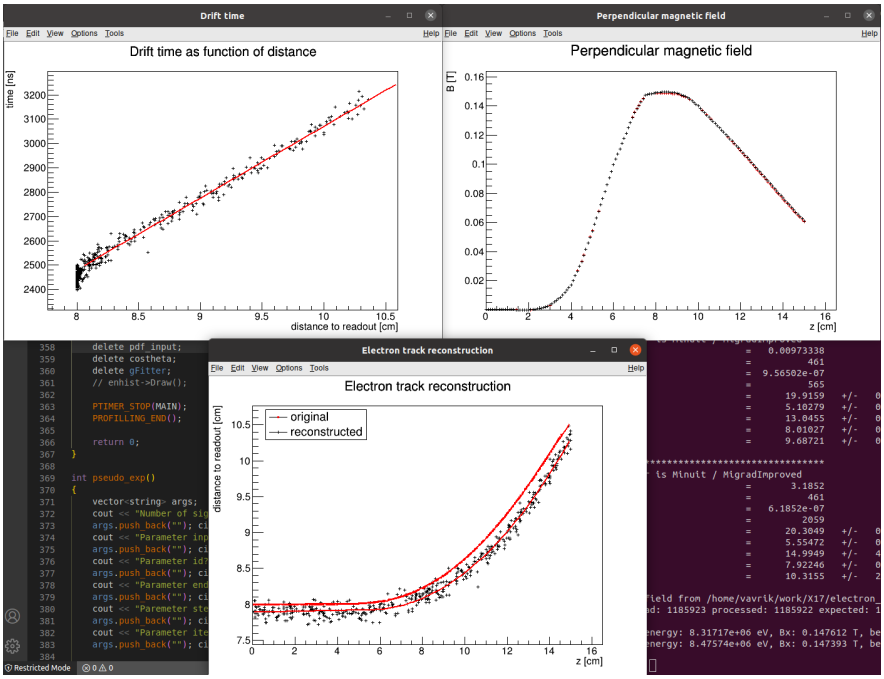

Figure 4.3: First attempt at a track reconstruction using only the drift velocity. Circle and Lines Fit in 2D. Swap for better image, correct coordinates.

The function defined in Equation 4.9 along with equations 4.11, 4.12, 4.18 and 4.19 derived using the continuity and smoothness conditions (combined with the relations for $z_{1,2}$) fully define our fitted function with parameters $r, x_{1,2}, z_{1,2}$. Some pictures of the fit on the tested track. Results of the fit. Again, the actual fit uses 8-z. Use GeoGebra schematics to generate a picture of 2D geometry.

Tested on a Runge-Kutta sample, and with microscopic tracks + map simulation. Preliminary 2D version (done) and complete 3D version. Geometry of the fit with its derivation.

4.2.2 Three-dimensional fit

Explain the geometry and least square method used for the 3D fit.

4.3 Runge-Kutta Fit

Single parameter fit with 4th order Runge-Kutta simulated track. Future testing with microscopic simulations and map simulation. Derivation of the geometry (least squares).

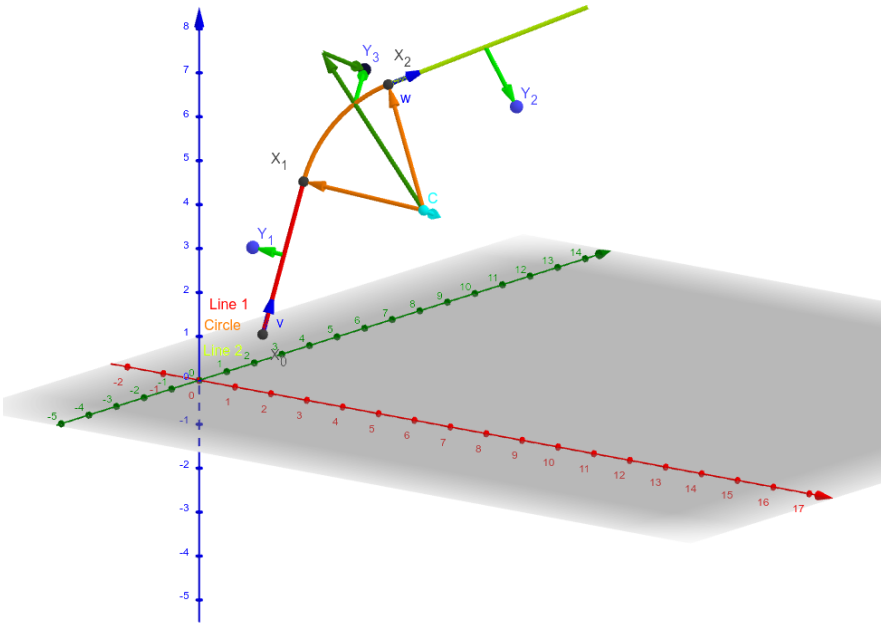

Figure 4.4: Circle and Lines Fit 3D geometry. Swap for better image.

Conclusion

Here or at the end of each section. Something about the future of this work?

Notes

General notes about the thesis:

- Check that all of the classes and other code are marked the same way in the text. I used italics somewhere, could use different font for this instead.
- Check unbreakable space in front of articles. Remove excessive article usage with proper nouns.
- Currently using margins for single-sided printing (bigger on the left side).
- Check that present tense is used
- American English quotation marks (") instead of British English (').
- Some of the overfull hbox warnings might change if duplex printing is used (they generate black rectangles on the edge of the page), leaving them be for now
- Check nobreakdash usage
- Check capitalized references (e.g., Figure, Section, Equation)

Random notes:

- Only electrons that start and end in the sector closer than 0.5 cm are used for reconstruction (newest version).

Future

Things planned for the future:

- Testing the reconstruction algorithm by measuring real particles with a known energy distribution.
- The **Fast Simulation with Ionization Electron Map** is planned for the future. It will use the HEED program [13] to simulate the primary particle and the Ionization Electron Map (see Section 3.2) to simulate the drift of secondary electrons. It should be significantly faster than the Microscopic Simulation but offer comparable precision since it will rely on an already simulated drift map. (Primary track simulated in HEED. Readout parameters by interpolating the map. Diffusion from the map for randomization.)
- Account for GEM, delta electrons, ...

- Likelihood approach instead of least squares (if it improves the reconstruction significantly), we should at least use a better method than taking the center of the TPC bin.

- More detailed electric field simulation (if needed, GEM will have more complex field)

Likelihood - inverse map

If we wanted to further improve this procedure, taking into account the whole map $\mathcal{M}$, we could make an "inverse map" from $\mathcal{R}$ to distributions on $\mathcal{D}$. We could achieve this by taking the normalized probability density of an electron with initial coordinates (x, y, z) having readout coordinates (x', y', t). If we fix (x', y', t), we get an unnormalized probability density $f(x, y, z) = \mathcal{M}_{(x,y,z)}(x', y', t)$ (assuming that all initial coordinates are a priori equally likely). This could potentially improve the discrete reconstruction if we take the mean value of this probability density across the pad and time bin

$$f_{\text{pad, bin}}(x, y, z) = \frac{1}{A_{\text{pad}} \Delta t_{\text{bin}}} \int_{\text{pad, bin}} \mathcal{M}_{(x,y,z)}(x', y', t) \mathrm{d}x' \mathrm{d}y' \mathrm{d}t \tag{4.20}$$

and using it for a likelihood fit instead of using least squares. This still assumes that all initial coordinates are equally likely which is clearly not the case for a primary particle track. In the future, we could even use the fast track simulation with the map (should be possible to make around 1000 tracks per minute per core with current settings), create a big set of tracks with reasonable parameters and use these to get an approximation of the probability distribution of the detector response. Some approximations would be necessary when interpreting the data to decrease the degrees of freedom of this distribution (we would have to pick a set of parameters and assume that some of them are independent). This could give us an idea about the best achievable resolution (how significantly will the detector response differ for a given change in energy). If the difference is significant, we could try to further improve the likelihood fit.

Bibliography

[1] Garfield++. https://garfieldpp.web.cern.ch/garfieldpp/. Accessed: 2023-05-18.

[2] Rene Brun and Fons Rademakers. Root — An Object Oriented Data Analysis Framework. *Nuclear Instruments and Methods in Physics Research Section A: Accelerators, Spectrometers, Detectors and Associated Equipment*, 389(1–2):81–86, Apr 1997. Proceedings AIHENP'96 Workshop, Lausanne, Sep. 1996, See also https://root.cern/, Paper published in the Linux Journal, Issue 51, July 1998.

[3] About MetaCentrum. https://metavo.metacentrum.cz/en/about/index.html, 2023. Accessed: 2024-11-27.

[4] M. E. Rose. Internal Pair Formation. *Phys. Rev.*, 76:678–681, Sep 1949.

[5] A. J. Krasznahorkay, M. Csatlós, L. Csige, Z. Gácsi, J. Gulyás, M. Hunyadi, I. Kuti, B. M. Nyakó, L. Stuhl, J. Timár, T. G. Tornyi, Zs. Vajta, T. J. Ketel, and A. Krasznahorkay. Observation of Anomalous Internal Pair Creation in ^{8}Be: A Possible Indication of a Light, Neutral Boson. *Physical Review Letters*, 116(4), January 2016.

[6] D.R. Tilley, J.H. Kelley, J.L. Godwin, D.J. Millener, J.E. Purcell, C.G. Sheu, and H.R. Weller. Energy levels of light nuclei A=8,9,10. *Nuclear Physics A*, 745(3):155–362, 2004.

[7] N. J. Sas, A. J. Krasznahorkay, M. Csatlós, J. Gulyás, B. Kertész, A. Krasznahorkay, J. Molnár, I. Rajta, J. Timár, I. Vajda, and M. N. Harakeh. Observation of the X17 anomaly in the ^{7}Li(p,$e^{+}e^{-}$)^{8}Be direct proton-capture reaction, 2022.

[8] A. J. Krasznahorkay, M. Csatlós, L. Csige, J. Gulyás, A. Krasznahorkay, B. M. Nyakó, I. Rajta, J. Timár, I. Vajda, and N. J. Sas. New anomaly observed in ^{4}He supports the existence of the hypothetical X17 particle. *Physical Review C*, 104(4), October 2021.

[9] D.R. Tilley, H.R. Weller, and G.M. Hale. Energy levels of light nuclei A = 4. *Nuclear Physics A*, 541(1):1–104, 1992.

[10] A. J. Krasznahorkay, A. Krasznahorkay, M. Begala, M. Csatlós, L. Csige, J. Gulyás, A. Krakó, J. Timár, I. Rajta, I. Vajda, and N. J. Sas. New anomaly observed in ^{12}C supports the existence and the vector character of the hypothetical X17 boson. *Phys. Rev. C*, 106:L061601, Dec 2022.

[11] F. Ajzenberg-Selove. Energy levels of light nuclei A = 11,12. *Nuclear Physics A*, 506(1):1–158, 1990.

[12] A. J. Krasznahorkay, M. Csatlos, L. Csige, J. Gulyas, M. Koszta, B. Szihalmi, J. Timar, D. S. Firak, A. Nagy, N. J. Sas, and A. Krasznahorkay. New evidence supporting the existence of the hypothetic X17 particle, 2019.

[13] I.B. Smirnov. Modeling of ionization produced by fast charged particles in gases. *Nuclear Instruments and Methods in Physics Research Section A: Accelerators, Spectrometers, Detectors and Associated Equipment*, 554(1):474–493, 2005.

Acknowledgments: Computational resources were provided by the e-INFRA CZ project (ID:90254), supported by the Ministry of Education, Youth and Sports of the Czech Republic.

List of Figures

List of Tables

List of Abbreviations

HEED High Energy Electro-Dynamics

IEAP CTU Institute of Experimental and Applied Physics, Czech Technical University in Prague

IPC Internal Pair Creation

MWPC Multi-Wire Proportional Chamber

OFTPC Orthogonal Fields TPC

TPC Time Projection Chamber

Tpx3 Timepix 3